Ultrasonics 76 (2017) 35–43

Contents lists available at ScienceDirect

Ultrasonics

journal homepage: www.elsevier.com/locate/ultras

Two-dimensional analytic modeling of acoustic diffraction for ultrasonic beam steering by phased array transducers

Tiansi Wang [a], Chong Zhang [b], Aleksandar Aleksov [c], Islam Salama [b], Aravinda Kar [a,d,*]

[a] CREOL, The College of Optics & Photonics, University of Central Florida, 4304 Scorpius Street, Orlando, FL 32816-2700, USA
[b] Intel – Assembly & Test Technology Development, 5000 W Chandler Blvd, Chandler, AZ 85226, USA
[c] Intel – Components Research, 5000 W Chandler Blvd, Chandler, AZ 85226, USA
[d] Mechanical and Aeronautical Engineering and Material Science Engineering Department, University of Central Florida, P.O. Box 162700, Orlando, FL 32816-2700, USA

ARTICLE INFO

Article history:
Received 21 June 2016
Received in revised form 1 December 2016
Accepted 3 December 2016
Available online 9 December 2016

Keywords:
Acousto-optic
Photo-acoustics
Ultrasonic beam steering
Phased array transducer

ABSTRACT

Phased array ultrasonic transducers enable modulating the focal position of the acoustic waves, and this capability is utilized in many applications, such as medical imaging and non-destructive testing. This type of transducers also provides a mechanism to generate tilted wavefronts in acousto-optic deflectors to deflect laser beams for high precision advanced laser material processing. In this paper, a theoretical model is presented for the diffraction of ultrasonic waves emitted by several phased array transducers into an acousto-optic medium such as TeO_2 crystal. A simple analytic expression is obtained for the distribution of the ultrasonic displacement field in the crystal. The model prediction is found to be in good agreement with the results of a numerical model that is based on a non-paraxial multi-Gaussian beam (NMGB) model.

Published by Elsevier B.V.

1. Introduction

Ultrasonic phased arrays consist of a number of individual elements of width and pitch that depend on the acoustic wavelength in the transducer medium. The width and pitch are generally comparable to or smaller than the ultrasonic half-wavelength each. This type of geometry offers a dynamic means of focusing and scanning the ultrasonic beam by modulating the time delay between the RF electronic excitation of the individual element. The phased array technology dominates in several important areas, such as radar, underwater acoustics, medical diagnostics, and therapeutic treatment. Much of the early work implemented one-dimensional arrays in medical devices for imaging applications [1–3]. Later two-dimensional arrays were implemented for volumetric imaging [4–6]. This initial success of the technology quickly spread into numerous sub-disciplines, such as pulse-echo imaging, Doppler techniques, sono-elastic imaging, computed tomography, and three-dimensional imaging [7,8]. Improvements were made in the therapeutic field by introducing intracavity phased arrays capable of increasing tissue temperature as a potential tool for prostate cancer treatment [9–11] and transskull therapy [12].

Non-destructive testing or evaluation (NDT or NDE) of materials, mainly in the field of nuclear inspection, utilizes the phased array transducer technology [13]. This technology enables acoustic imaging for NDE and locating the position of flaws quickly and accurately. Other notable endeavors include the time-reversal processing [5], and self-focusing techniques [6]. These efforts have provided a variety of NDE tools for industrial applications to image flaws or detect defects by swiftly scanning an ultrasonic beam over the material of interest [3]. The sensitivity and efficiency of the ultrasonic diagnostic and inspection are greatly enhanced by the phased array technique due to the constructive or destructive interference as well as the diffraction of the ultrasonic waves.

The tremendous success of the ultrasonic diagnostic technology in the medical and NDE fields sparked considerable interest for possible applications in optics and photonics since 1960s [14] after the invention of lasers. Acousto-optic scanning and deflection (AOSD) devices have been produced for a variety of laser applications such as detection, modulation, or filtering of coherent light. The operating principle of these devices include modulation of the refractive index of an acousto-optic medium using acoustic waves to generate a transparent dynamic volume phase grating that deflects an incident laser beam. This type of acousto-optic deflectors (AODs) has been used in many applications such as laser marking, micromachining, patterning and direct writing. Galvo scanners are traditionally used to direct laser beams to different locations on a workpiece using two mirrors. The mechanical motion of x-y mirrors in the scanner affects the accuracy of beam positioning and repeatability in high-volume manufacturing. Ultrasonic beam steering without any moving optical component

* Corresponding author at: CREOL, The College of Optics & Photonics, University of Central Florida, P.O. Box 162700, Orlando, FL 32816-2700, USA.
E-mail address: akar@creol.ucf.edu (A. Kar).

http://dx.doi.org/10.1016/j.ultras.2016.12.005
0041-624X/Published by Elsevier B.V.

is necessary to overcome the limitations of conventional scanning technology. The ability to steer ultrasonic beam in different directions within the acousto-optic crystal using phased array transducers provides a unique device for flexible and high speed deflection of laser beams with high precision and accuracy.

The fundamental aspect of this new device is the capability to steer ultrasonic waves inside the crystal using phased array transducers. The diffraction of the waves is studied to analyze the formation of the zeroth order diffraction lobe as the steered ultrasonic beam. The ultrasonic displacement vector field generated by an immersion piston transducer can be calculated using the Rayleigh-Sommerfeld integral (RSI) model for liquid [15]. In solid media, on the other hand, Vezzetti's model [16] is applied to determine the ultrasonic displacement vector field generated by a contact piston transducer, because this model accounts for the Christoffel equation of motion. This solid media model yields an integral equation for the displacement vector field by the method of angular spectrum. Schmerr [17] simplified Vezeetti's model to obtain an explicit expression that resembles the Rayleigh-Sommerfeld diffraction integral for the displacement field and, therefore, Schmerr's model is called the modified Rayleigh-Sommerfeld integral (mRSI) model.

NMGB model [18] optimizes several parameters to evaluate mRSI, yielding a fast numerical method for determining the displacement of atoms due to acoustic waves. The acoustic intensity distribution causes periodic oscillation of the atoms by displacing them around their equilibrium positions and thus induces strain in the medium. In AOD studies, however, the acoustic strain-induced index modulation is calculated and this modulation is applied to Maxwell's equation for analyzing the laser beam propagation through the AOD to determine the deflection angle of the laser beam and the diffraction efficiency. The strain, which is given by the spatial derivatives of the displacement vector, has to be determined by a numerical method such as finite difference approximation if the discrete outputs of the NMGB model are utilized. So the calculation of strain would be erroneous and time-consuming due to the numerical computation of the derivatives.

Fourier model is developed in this study to obtain an analytic expression for the displacement vector so that the spatial derivatives of the vector can be evaluated analytically. Therefore, the strain can be represented by an analytic expression that will enable accurate and rapid computation of the strain. Filon model, on the other hand, provides an analytic expression for the displacement vector as a series from which the strain can be determined analytically. However, the Filon model takes longer computational time than the Fourier model. The Filon and NMGB models are used to verify the Fourier model and then the subsequent results are obtained from the Fourier model.

Since TeO_2 is a good AOD material for lasers of wavelength 0.35–5.0 μm, the Fourier and Filon models are developed in this paper for the displacement field in TeO_2 by applying the mRSI model to ultrasonic linear phased array transducers. This paper begins by presenting a theoretical background in Section 2 as a foundation for the two models. These two new models are validated in Section 3 by comparing their results to that of the NMGB model and then the profile of the displacement field is analyzed using the Fourier model for various ultrasonic beam steering angles. Finally, the results are summarized and discussed in Section 4.

2. Theoretical background

Conventional AODs are operated with a single transducer, or an array of transducers assembled in the planar or stepped configuration [14]. The performance of single-transducer AODs is limited by the applied radiofrequency (RF) power, narrow bandwidth, small deflection angle and narrow scan angle of the laser beam, and low diffraction efficiency. Phased array transducers are used to improve the performance of AODs. Each transducer is operated with relative time delay in the applied RF power to generate phase-shifted ultrasonic waves. These waves form a tilted wavefront in the AOD medium due to the diffraction of the waves. The interaction of a laser beam with the tilted wavefront improves the deflection angle and diffraction efficiency [19]. Conventional phased array AODs are, however, operated with fixed time delays, and therefore, the ultrasonic wavefronts cannot be steered at any arbitrary angle for a given AOD. To achieve flexibility in the ultrasonic beam steering, the time delays of the transducers can be varied during the operation of the AOD. This type of beam steering or focusing technique produces a tilted ultrasonic diffraction pattern with the zeroth order diffraction lobe pointing in the principal direction z_s at the steering angle θ_s as shown in Fig. 1a [19,20].

In this paper, the mathematical formulation to analyze the beam steering is based on Nakahata and Kono's [21] three-dimensional model for ultrasonic wave patterns in solids due to phased array transducers. Their single-transducer model is applied to multiple phased array transducers in this study for two-dimensional wave patterns. The geometry of the AOD medium is presented in Fig. 1a with transducers that are infinitely long along the y axis. So the displacement of the atoms at any point P(x,z) in the AOD medium for unit length in the y direction is given by the following expression for longitudinal ultrasonic waves in the medium.

$$\vec{U}(x,z) = \frac{1}{2\pi\rho}\sum_{m=1}^{M}\frac{P_m}{c_{lm}^2}\int_{-\infty}^{\infty} D(\theta(x_m))\vec{d}_p(x_m) \times \frac{\exp[(i\kappa_m - \alpha_m)r_m]}{r_m} Rect\left(\frac{x_m - x_{cm}}{2a_m}\right) exp(i\Delta\phi_m)dx_m \quad (1)$$

Here ρ is the density of the AOD medium and c_{lm} represents the speed in this medium for the longitudinal ultrasonic waves emitted by the m-th transducer. Since the speed depends on the ultrasonic frequency, the effect of operating the transducers at different frequencies can be analyzed by selecting the value of c_{lm} corresponding to each frequency. p_m is the pressure exerted on the AOD medium by the m-th transducer. $\kappa_m(=\omega_m/c_{lm})$ and α_m are the wave number and attenuation coefficient of the ultrasonic wave in the medium, respectively, where ω_m is the angular frequency of the waves, due to m-th transducer. M is the total number of transducers. The distance between the point P(x,z) and an arbitrary point $B(x_m,0)$ on the m-th transducer is denoted by

$$r_m = BP = \sqrt{(x - x_m)^2 + z^2} \quad (2)$$

and the rectangular function is defined as

$$Rect\left(\frac{x_m - x_{cm}}{2a_m}\right) = \begin{cases} 1, & \text{for } x_{cm} - a_m \leqslant x_m \leqslant x_{cm} + a_m \\ 0, & \text{otherwise} \end{cases} \quad (3)$$

where a_m is the half-width of the m-th transducer, which allows to study the effect of the transducer size variation on the ultrasonic wave pattern in the medium, and x_{cm} is the x-coordinate of the mid-point on the m-th transducer. The directivity function for the m-th transducer, $D(\theta_m)$, is given by

$$D(\theta(x_m)) = \frac{c_m^2\left(\frac{1}{2}c_m^2 - \sin^2\theta(x_m)\right)\cos\theta(x_m)}{2(\sin^2\theta(x_m) - c_m^2/2)^2 + \frac{1}{2}\sin^2(2\theta(x_m))\sqrt{c_m^2 - \sin^2\theta(x_m)}} \quad (4)$$

where $\theta(x_m)$ is the angle between the line BP and the normal to the surface of the m-th transducer at an arbitrary point x_m, and

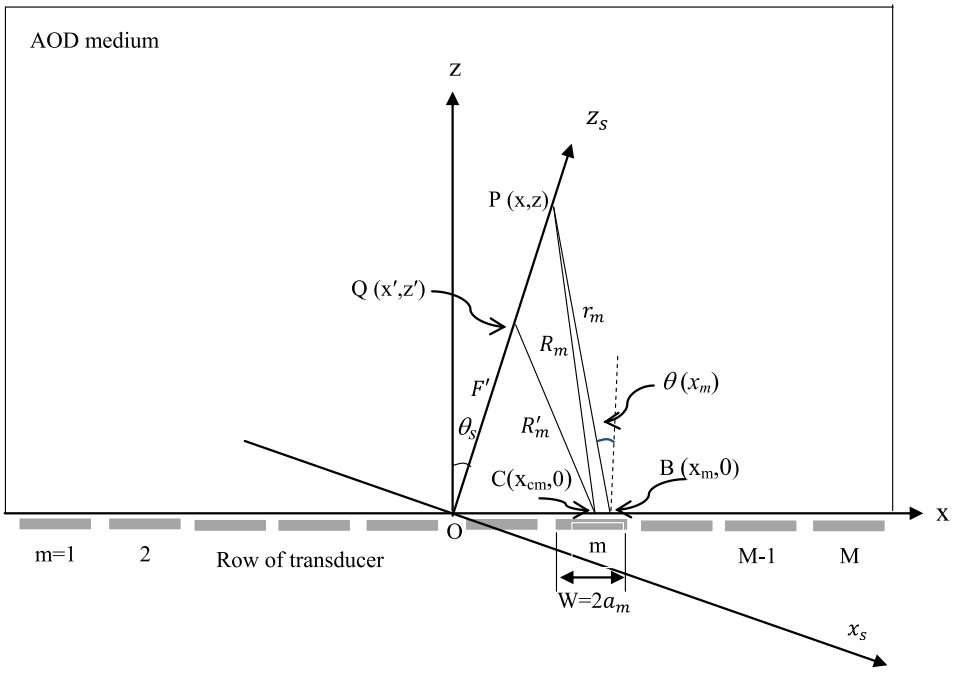

Fig. 1a. Geometry of the AOD medium and piezoelectric transducers for ultrasonic beam steering.

$c_m = c_{lm}/c_{tm}$ where c_{tm} is the speed of ultrasonic shear waves in the AOD medium due to the m-th transducer. The polarization vector for the m-th transducer, $\vec{d}_p(x_m)$, is given by

$$\vec{d}_p(x_m) = \frac{x - x_m}{r_m}\hat{x} + \frac{z}{r_m}\hat{z} \tag{5}$$

where $\hat{x}$ and $\hat{z}$ are the unit vectors in the x and z directions respectively. The phase shift $\Delta\phi_m$ represents the ultrasonic phase difference between the center of each transducer element, such as C (x_{cm},0) and the center of the entire transducer array, such as O (0,0), in Fig. 1a. This phase shift is related to the time delays for ultrasonic waves arriving at point Q(x′,z′) from points C(x_{cm},0) and O(0,0), i.e., $\Delta\tau_m = (F' - R'_m)/c_{lm}$, where Q is the point of focus at a distance F' from the point O, and R'_m is the distance CQ [21,22]. Applying the cosine law of triangle to the triangle QOC, the relationship between the phase shift and time delay can be expressed as

$$\Delta\phi_m = 2\pi F_m \Delta\tau_m = \frac{2\pi}{\Lambda_m} F'[1 - \{F'^2 + x_{cm}^2 - 2F'x_{cm}\sin\theta_s\}^{1/2}] \tag{6}$$

where F_m and Λ_m are the frequency and wavelength of the ultrasonic waves in the AOD medium, respectively, for the m-th transducer. In this study, all of the transducers are considered to emit ultrasonic waves of the same frequency and wavelength. x_{cm} represents the coordinate value of the center of m-th transducer, i.e., x_{cm} is negative for the transducers lying on the –x axis. The steering angle θ_s is considered positive when measured from the z axis in the clockwise direction.

2.1. Fourier model for a linear phased array transducer

This model is developed by carrying out the integration in Eq. (1) analytically, and the model is named after Fourier because the analytic result involves the sine and cosine functions. When the width of a transducer, $W_m = 2a_m$, is very small, the variation of the directivity function and the polarization vector, $\vec{d}_p(x_m)$, at various points within a given transducer would be very small. Therefore, evaluating these two variables at x_{cm}, i.e., taking $D(\theta(x_m)) \approx D(\theta(x_{cm}))$ and $\vec{d}_p(x_m) \approx \vec{d}_p(x_{cm})$, Eq. (1) can be simplified as

$$\vec{U}(x,z) = \sum_{m=1}^{M} A_m \int_{x_{cm}-a_m}^{x_{cm}+a_m} \frac{\exp(iK_m r_m)}{r_m} dx_m \tag{7}$$

where $A_m = \frac{1}{2\pi\rho}\frac{p_m}{c_{lm}^2} D(\theta(x_{cm}))\vec{d}_p(x_{cm}) exp(i2\pi F_m \Delta\tau_m)$ and $K_m = \kappa_m + i\alpha_m$. Using Eq. (2) to change the variable of integration from x_m to r_m, Eq. (7) can be written as

$$\vec{U}(x,z) = -\sum_{m=1}^{M} A_m \int_{b_l}^{b_u} \frac{\exp(iK_m r_m)}{x - x_m} dr_m \tag{8}$$

where $b_l = \sqrt{z^2 + [x - (x_{cm} - a_m)]^2}$ and $b_u = \sqrt{z^2 + [x - (x_{cm} + a_m)]^2}$. Noting that the oscillating exponential factor $\exp(ik_m r_m)$ in the integrand of Eq. (8) varies rapidly compared to the denominator x-x_m, and x-$x_m \approx x$-x_{cm} for small widths of the transducers, Eq. (8) yields

$$\vec{U}(x,z) = -\sum_{m=1}^{M} \frac{A_m}{iK_m} \frac{\exp(iK_m b_u) - \exp(iK_m b_l)}{x - x_{cm}} \text{ for } x \neq x_{cm} \tag{9}$$

For the case of, $x = x_{cm}$, L'Hospital's rule is applied to Eq. (8) by taking the limit as $x \to x_{cm}$ to obtain the following expression for the displacement vector field.

$$\vec{U}(x,z) = 2\sum_{m=1}^{M} A_m \frac{a_m}{\sqrt{z^2 + a_m^2}} \exp(iK_m\sqrt{z^2 + a_m^2}) \text{ for } x = x_{cm} \tag{10}$$

Eqs. (9) and (10) will be used to analyze the ultrasonic beam steering in the AOD medium due to phase modulation of the piezoelectric transducers.

2.2. Filon model for a linear phased array transducer

This model is named after Filon because the integration in Eq. (1) is carried out following Filon's quadrature method for trigonometric integrals [23] of the form:

$$\int_{X_l}^{X_u} \psi'(x)\sin(kx)dx \tag{11}$$

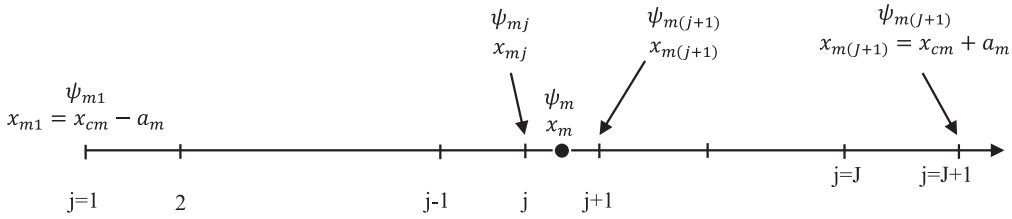

Fig. 1b. Nodal points on the m-th transducer for Filon model.

In this method, the integral is represented by a sum of integrals over small intervals within the range of integration $[X_l, X_u]$, and the function $\psi'(x)$ is approximated as a polynomial, such as a quadratic function [23] or a linear function [24], to evaluate the integral analytically in each interval.

To apply Filon's method, Eq. (2) is substituted into Eq. (7) to obtain the following expression:

$$\vec{U}(x,z) = \sum_{m=1}^{M} \frac{A_m}{z} \int_{x_{cm}-a_m}^{x_{cm}+a_m} \frac{\exp(iK_m z\psi(x_m))}{\psi(x_m)} dx_m \tag{12}$$

where

$$\psi_m = \sqrt{1 + \left(\frac{x - x_m}{z}\right)^2} \tag{13}$$

The interval of integration, $[x_{cm} - a_m, x_{cm} + a_m]$, is divided into J number of equal intervals with $j = 1$ for the first point at the lower limit of the integration, i.e., $x_{m1} = x_{cm}$-a_m and $j = J + 1$ for the last point at the upper limit of the integration, i.e., $x_{m(J+1)} = x_{cm} + a_m$ as shown in Fig. 1b, and the width of each interval is $\Delta x_m = x_{m(j+1)} - x_{mj} = \frac{2a_m}{J}$. The integral in Eq. (12) can be written as a sum of J number of integrals as follows:

$$\vec{U}(x,z) = \sum_{m=1}^{M} \frac{A_m}{z} \sum_{j=1}^{J} \int_{x_{mj}}^{x_{m(j+1)}} \frac{\exp(iK_m z\psi(x_m))}{\psi(x_m)} dx_m \tag{14}$$

To evaluate the integrals in Eq. (14), $\psi(x_m)$ is fitted as a straight line in each interval of integration, $x_{mj} \leqslant x_m \leqslant x_{m(j+1)}$. It should be noted that the coefficient of the sinusoidal function, i.e., $\psi'(x)$ in Eq. (11), is approximated as a polynomial or a linear function in each interval of integration in the original Filon method. This original approach is modified in this study by approximating the denominator, $\psi(x_m)$, as a straight line in each interval of integration, i.e.,

$$\psi(x_m) = \psi_{mj} + \Delta\psi_{mj}\xi_m \tag{15}$$

where $\psi_{mj} = \psi(x_{mj})$, $\Delta\psi_{mj} = \psi_{m(j+1)} - \psi_{mj}$ and ξ_m is the normalized distance within the m-th transducer given by $\xi_m = \frac{x_m - x_{mj}}{\Delta x_m}$. ψ_{mj} and $\psi_{m(j+1)}$ are specified in Fig. 1b and these two variables can be determined using Eq. (13) such as $\psi_{mj} = \sqrt{1 + [(x - x_{mj})/z]^2}$. Substituting Eq. (15) into Eq. (14), the total displacement vector can be written as

$$\vec{U}(x,z) = \sum_{m=1}^{M} \frac{A_m}{z} \sum_{j=1}^{J} \Delta x_m \int_0^1 \frac{\exp(iK_m z(\psi_{mj} + \Delta\psi_{mj}\xi_m))}{\psi_{mj} + \Delta\psi_{mj}\xi_m} d\xi_m \tag{16}$$

and Eq. (16) is evaluated for the following two cases.

(i) When $\Delta\psi_{mj} = 0$, the integrand in Eq. (16) is independent of ξ_m and the following expression is obtained for the displacement vector.

$$\vec{U}(x,z) = \sum_{m=1}^{M} \frac{2A_m a_m}{zJ} \sum_{j=1}^{J} \frac{\exp(iK_m z\psi_{mj})}{\psi_{mj}} \tag{17}$$

(ii) When $\Delta\psi_{mj} \neq 0$, the change of variable, $\beta_m = \psi_{mj} + \Delta\psi_{mj}\xi_m$, is applied to Eq. (16) to obtain the following expression:

$$\vec{U}(x,z) = \sum_{m=1}^{M} \frac{2A_m a_m}{zJ} \sum_{j=1}^{J} \frac{1}{\Delta\psi_{mj}} \int_{\psi_{mj}}^{\psi_{m(j+1)}} \frac{\exp(iK_m z\beta_m)}{\beta_m} d\beta_m \tag{18}$$

which yields the following result in terms of the cosine and sine integrals [25], e.g., Ci(Z) and Si(Z) of an arbitrary argument Z, respectively.

$$\vec{U}(x,z) = \sum_{m=1}^{M} \frac{2A_m a_m}{zJ} \sum_{j=1}^{J} \frac{1}{\Delta\psi_{mj}} [\{Ci(K_m z\psi_{m(j+1)}) - Ci(K_m z\psi_{mj})\} + i\{Si(K_m z\psi_{m(j+1)}) - Si(K_m z\psi_{mj})\}] \tag{19}$$

Eqs. (17) and (19) are used to calculate the displacement vector and the accuracy is verified by comparing with the results of the Fourier and NMGB models.

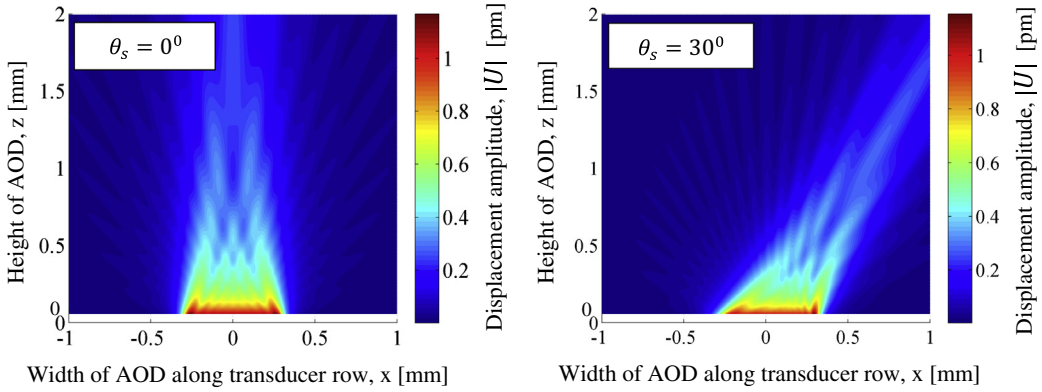

Fig. 2. Two-dimensional amplitude of the ultrasonic displacement field $|U|$ in the AOD medium based on NMGB model for two beam steering angles.

3. Numerical results and discussion

TeO_2 is the acousto-optic medium for numerical simulation in this study with a row of M = 22 piezoelectric transducers. Each transducer is operated at the ultrasonic frequency of F = 75 MHz each, and at this frequency, the speeds of S and L waves are c_{sm} = 616 ± 10 m/s c_{lm} = 4202 ± 10 m/s, respectively [26]. For the L waves, the ultrasonic wavelength and wavenumber are $\Lambda = 56\ \mu m$ and $\kappa_m = 1.12 \times 10^5\ m^{-1}$, respectively. The width of each transducer element is W = 20.8 μm which yields the half-width a_m = 10.4 μm. The row of the transducers and the height of the AOD medium are aligned with the x and z axes, respectively, with the origin of this coordinate system lying at the center of the transducer row of pitch S = Λ/2 = 56 μm as shown in Fig. 1a. For the computation in the Filon model, the total number of intervals $J = 2$, that yields the integration step Δx_m = 10.4 μm, which is approximately Λ/5 and sufficiently small to resolve the ultrasonic wavefront for beam steering studies. The pressure exerted on the

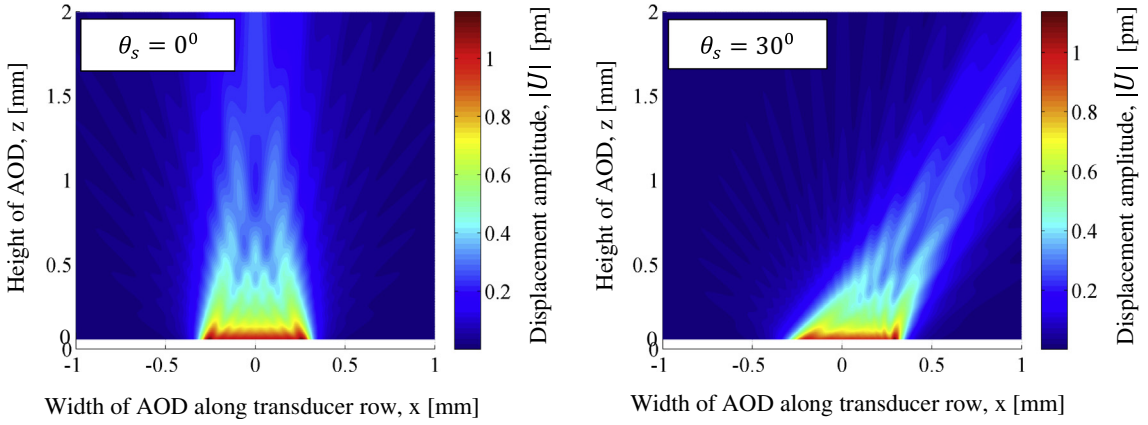

Fig. 3. Two-dimensional amplitude of the ultrasonic displacement field |U| in the AOD medium based on Fourier model for two beam steering angles.

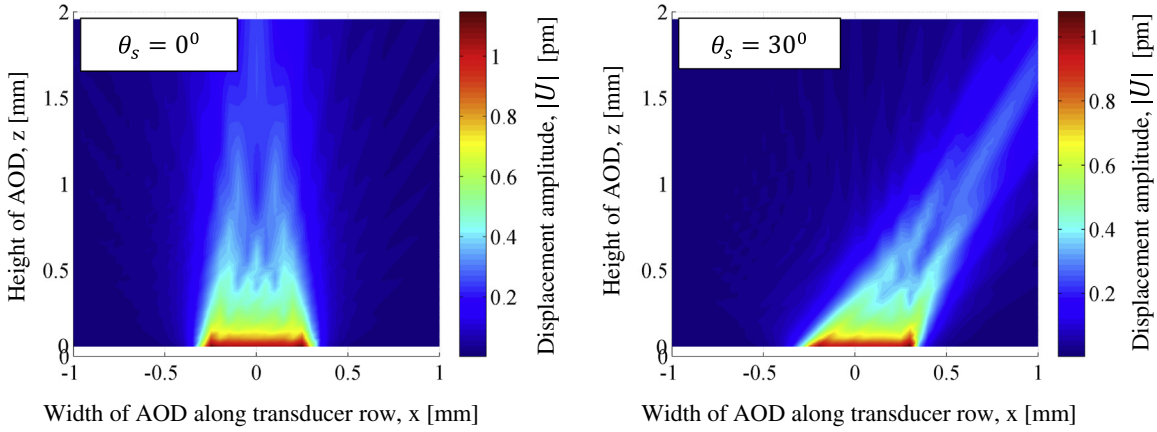

Fig. 4. Two-dimensional amplitude of the ultrasonic displacement field |U| in the AOD medium based on Filon model for two beam steering angles.

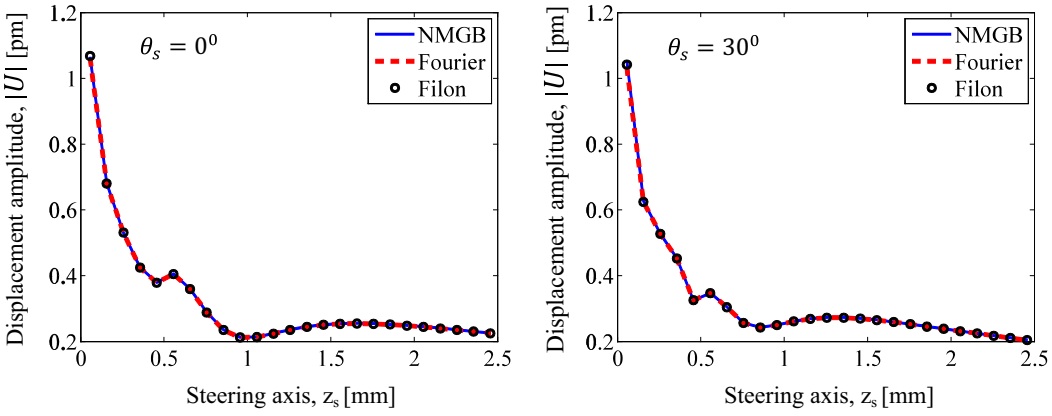

Fig. 5. Comparison of one-dimensional amplitude of the ultrasonic displacement field |U| in the AOD medium based on NMGB, Fourier and Filon models for two steering angles to verify the accuracy of the models.

AOD medium by each transducer is taken as p_m = 1 N/mm^2 and the distance of the point of focus from the origin of the x-z coordinate system is considered to be very large at F = 1 km.

The accuracy of the ultrasonic wave model plays an important role in the design of acousto-optic deflector and the investigation of acousto-optic interactions. So the ultrasonic displacement fields obtained from the NMGB [18] are used to verify the accuracy of the Fourier analytical model and the Filon numerical model for two values of the beam steering angle at the ultrasonic central frequency of F = 75 MHz. Figs. 2–4 show the results of the NMGB, Fourier and Filon models, respectively, which represent the two-dimensional amplitudes of the ultrasonic displacement field $|U|$ for the beam steering angles of $\theta_s = 0^\circ$ and 30° in each figure. These results indicate that the two models of this study are in good agreement with the NMGB model.

The models are also compared along the ultrasonic beam steering axis inside the TeO_2 crystal. Each model yields the displacement vector $\vec{U}$. The scalar magnitude of this vector is $U = \sqrt{\vec{U} \cdot \vec{U}}$, which is a complex variable in this study. The amplitude of U, which is given by the modulus $|U| = \sqrt{UU^*}$, where U∗ is the complex conjugate of U, is plotted in Fig. 5 for the steering angles θ_s = 0° and 30°, indicating that the three models are in good agreement. The curves clearly distinguish the ultrasonic wave propagation domain into two sections, representing the near field and far field regions of the diffraction pattern. The near field regions extend to approximately 56 μm and 1.0 mm from the z_s = 0 surface (Fig. 1a) for θ_s = 0° and 30°, respectively, before the development of the far-field region. For phased array transducers emitting ultrasonic waves of a single frequency, the near field region is char-

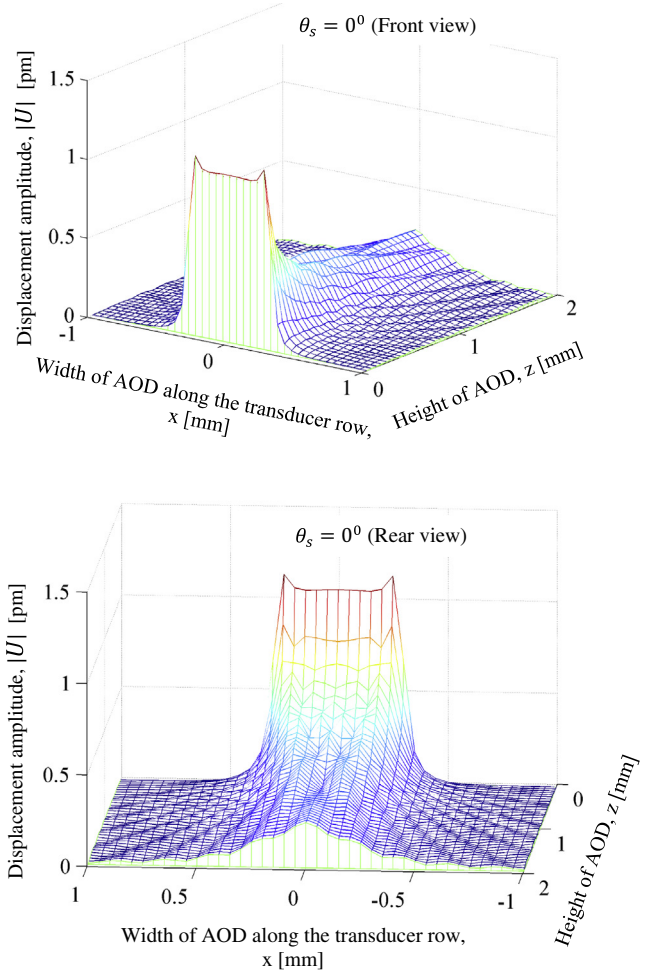

Fig. 6. Front and rear views of three-dimensional amplitude of the ultrasonic displacement field $|U|$ in the AOD medium based on Fourier model for the steering angle of 0°.

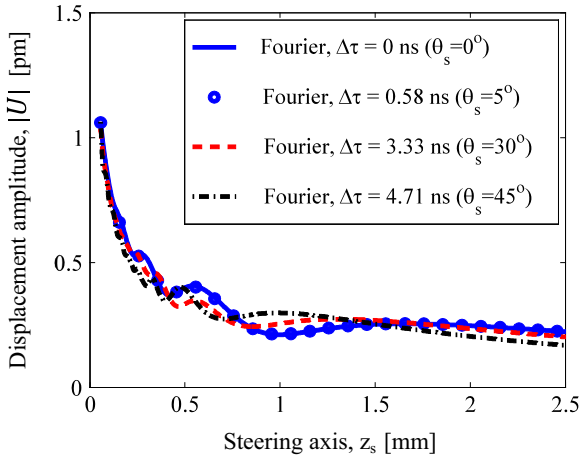

Fig. 7. Comparison of one-dimensional amplitude of the displacement field $|U|$ in the AOD medium based on Fourier model to study the effect time delay on the amplitude profile.

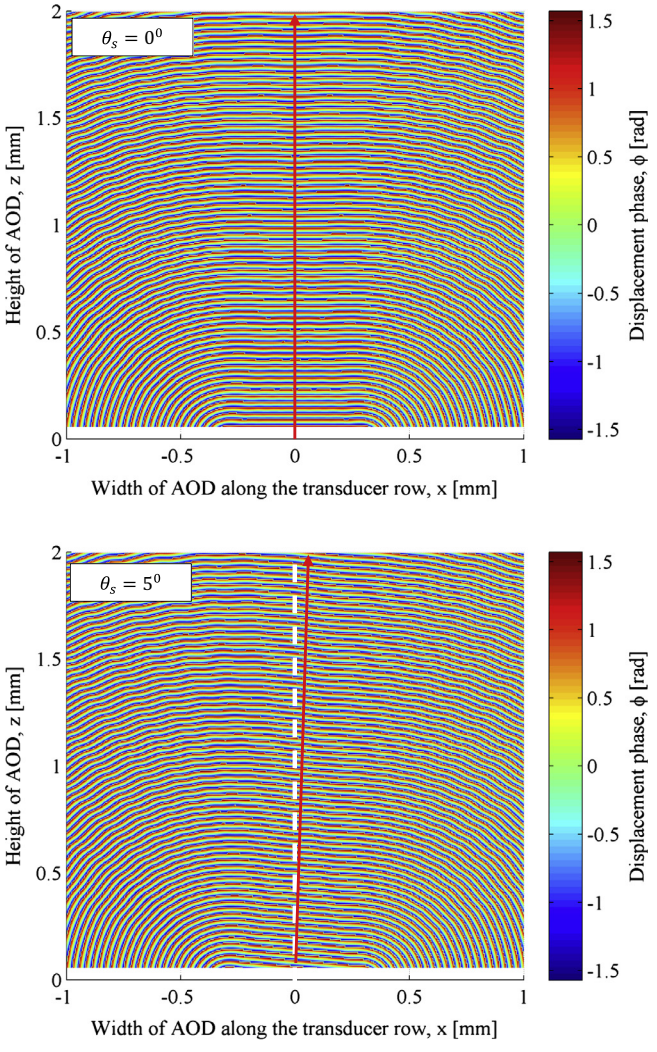

Fig. 8. Phase plot of the ultrasonic displacement field $|U|$ in the AOD medium based on Fourier model for two beam steering angles.

acterized by the amplitude of the field varying rapidly with maximum and minimum values. The reason for this type of variation in the amplitude is that the phase of the waves, which arrive from different regions of the transducer array, vary rapidly from point to point near the transducer plane (z = 0 in Fig. 1a) [22], resulting in maximum and minimum amplitudes due to constructive and destructive interferences respectively. The amplitude of the ultrasonic field is nearly constant over a certain range of the far field region, and this region is generally preferred for AOD applications because the uniform acoustic amplitude produces a phase grating of constant refractive index amplitude. Due to good agreements between the NMGB, Fourier and Filon models, and the simplicity of the Fourier model, the following results are obtained using the Fourier model.

Fig. 6 is a three-dimensional view showing the amplitude $|U|$ along the x and z directions in the TeO_2 medium based on Fourier model for the beam steering angle $\theta_s = 0°$. The ultrasonic wave propagation is calculated from one wavelength above the transducer plane, i.e., from z = 56 μm. For $\theta_s = 0°$, the amplitude profile is symmetric about the $x = 0$ line as the wave propagates in the z direction. Fig. 6 shows the front and rear views of the amplitude profile. Near the transducer plane, i.e., close to the z = 0 plane, the front view of the amplitude profile exhibits a rectangular diffraction pattern consisting of peaks at the two edges of

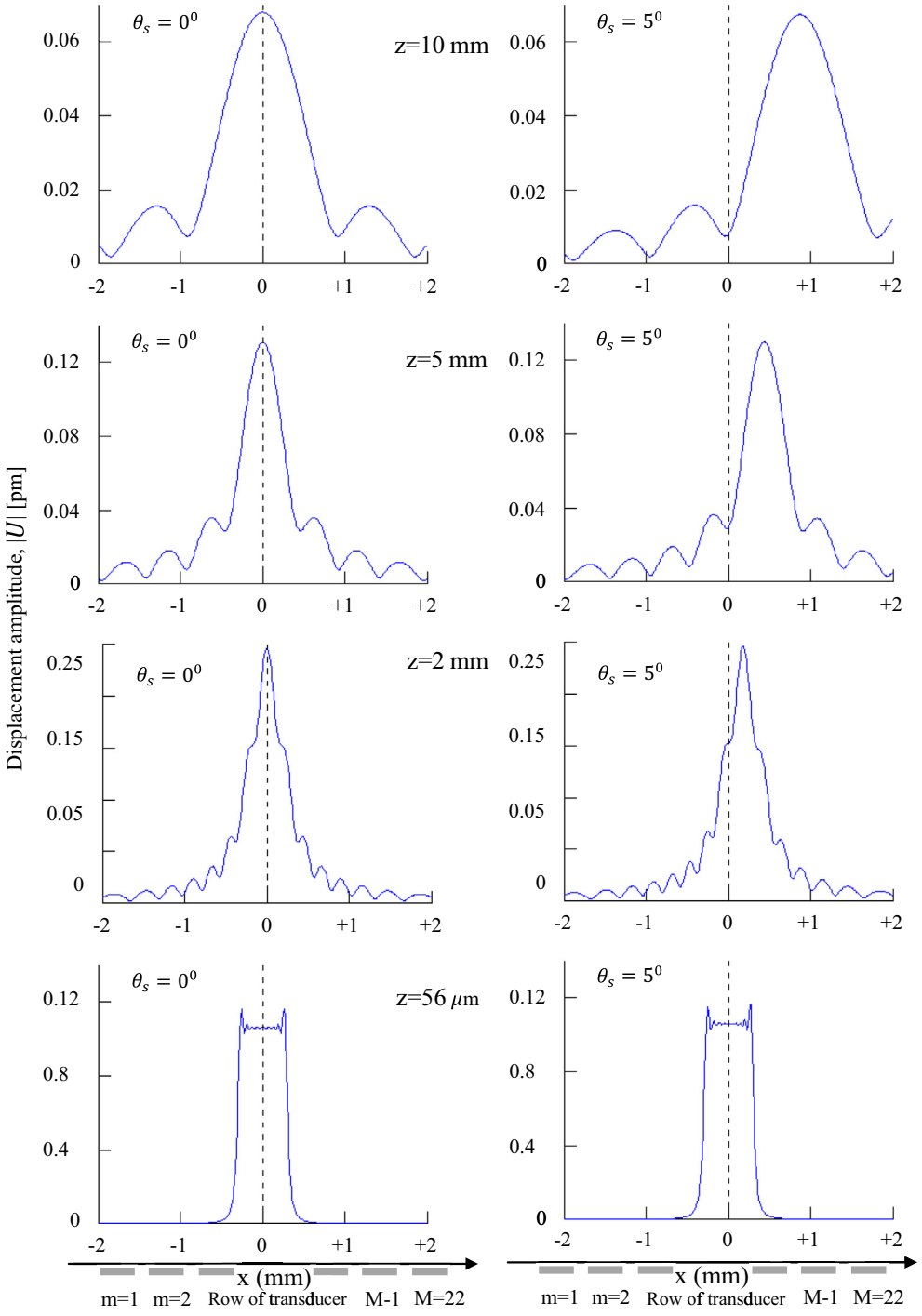

Fig. 9. Effect of diffraction on the evolution of the amplitude of the ultrasonic displacement field $|U|$ at different heights in the AOD medium based on Fourier model for two beam steering angles.

the rectangle and oscillations of very small amplitude between the edges. This pattern is similar to the profile produced by Gibbs' phenomenon when a rectangle function is synthesized using a Fourier series. The synthesized function overshoots at the edges of the rectangle function and oscillates between the edges. In this study, each transducer emits ultrasonic waves as a rectangle function, and the resulting diffraction pattern near the transducer plane is denoted as Gibbs' profile. This profile spreads and the overall amplitude decreases as the waves propagate in the x and z directions. Gibbs' profile transforms into the Fresnel diffraction pattern as shown in the rear view at z = 2 mm.

The effect of phase shift or time delay on the amplitude profile is studied in Fig. 7. The time delays between two neighboring transducers are taken as $\Delta\tau$ = 0 ns, 0.58 ns, 3.33 ns and 4.71 ns, which correspond to the steering angles θ_s = 0°, 5°, 30° and 45°, respectively. Due to different steering angles and, correspondingly, different time delays, the phase characteristics of the ultrasonic waves arriving at the same observation position P(x,z) [Fig. 1a] from the transducers would be different. Consequently, the peaks and valleys, which are formed in the resultant displacement field due to the interference of the waves, will be different for these cases as shown in Fig. 7. However, the length of the near field is approximately 1 mm for the three cases, and the amplitude is nearly constant in the far field region for the steering angles up to 30°.

The phase plots, i.e., $\tan^{-1}(U_i/U_r)$, where U_i and U_r are the imaginary and real parts of U respectively, are presented in Fig. 8 for the steering angles θ_s = 0° and 5° to show that the wavefronts also tilt by the same angle as θ_s. The wavefronts are formed due to the interference of the waves emitted by the phased array transducers. The main, i.e., the zeroth order, diffraction lobe coincides with the steering axis z_s corresponding to the steering angles θ_s = 0° and 5°, and the side lobes, i.e., the higher order diffraction pattern is formed in the transverse direction of the z_s axis. The tilted wavefront implies slanted displacement field that produces an oblique phase grating in the AOD medium. This type of oblique phase gratings can be utilized to increase the deflection angles of laser beams in AODs.

The characteristics of the main and side diffraction lobes are examined in Fig. 9, which shows the amplitude of the ultrasonic displacement field along x-axis, for the steering angles θ_s = 0° (left) and 5° (right) at different distances, z = 56 μm, 2 mm, 5 mm and 10 mm, from the transducer plane. The common diffraction features can be observed in both groups of the amplitude profile [27]. Near the source, i.e., close to the transducer plane, typical diffraction pattern of rectangular shape is observed and then the shape changes to the Fresnel diffraction profile in the near-field region. This pattern ultimately evolves into the Fraunhofer profile in the far-field region. In the case of $\theta_s = 0°$, the amplitude profiles are symmetric about the z axis since this axis coincides with the steering axis (z_s). On the other hand, the profiles are asymmetric about the z axis in the case of $\theta_s = 5°$ because the z and z_s axes do not coincide. Gibbs' profile is observed at z = 56 μm, which is near the transducer plane, and the Fresnel diffraction pattern is observed at a distance of z = 10 mm, indicating the existence of near-field diffraction effect over a large distance in the AOD medium. However, the peak of the main lobe shifts to the right, which indicates that the peak lies on the steering axis z_s.

4. Summary and conclusion

Two models called Fourier and Filon models have been developed to analyze the performance of phased array transducers for producing ultrasonic displacement field in AOD media. The Fourier model provides analytic solution for the displacement field, while the Filon model involves numerical integration of the diffraction integral to express the displacement field as a series. The accuracy of these two models is found to be excellent by comparing the results with the NMGB model. By varying the phases of the ultrasonic waves emitted by the transducers, i.e., by operating the transducers at different time delays, the waves can be caused to interfere to produce a diffracted wave pattern in a predetermined direction called the beam steering axis. This type of beam steering can be utilized to scan ultrasonic waves inside materials for nondestructive testing. The amplitude of the composite wave exhibits a rapidly varying wavy characteristic in the near field region and an almost constant value in the far field region. Therefore, nonperiodic and periodic phase gratings would be formed in the near and far field regions, respectively. So the beam steering effect and the far field region can be utilized in AODs to achieve large deflection angles for laser beams. Since the phase grating region extends over a certain volume inside the AOD medium and is primarily affected by the main lobe of the diffraction pattern, the locus of the main lobe is important in AOD applications. The peak of the main lobe is found to lie on the steering axis and the width of the lobe increases along this axis.

Acknowledgments

This work was supported by Semiconductor Research Corporation (SRC) and Intel Corporation.

References

[1] C.S. De Silets, Transducer Arrays Suitable for Acoustic Imaging Ph.D. Dissertation, Stanford University, Stanford, California, 1978.
[2] A. Macovski, Ultrasonic imaging using arrays, Proc. IEEE 67 (1979) 484–495.
[3] O.T. Von Ramm, S.W. Smith, Beam steering with linear arrays, IEEE Trans. Biomed. Eng. BME-30 (1983) 438–452.
[4] S.W. Smith, H.G. Pavy Jr., O.T. Von Ramm, High-speed ultrasound volumetric imaging system—Part I: transducer design and beam steering, IEEE Trans. Ultrason. Ferroelectr. Frequency Control 38 (1991) 100–108.
[5] O.T. Von Ramm, S.W. Smith, H.G. Pavy Jr., High-speed ultrasound volumetric imaging system—Part II: parallel processing and image display, IEEE Trans. Ultrason. Ferroelectrics Frequency Control 38 (1991) 109–115.
[6] D.H. Turnbull, S.F. Foster, Beam steering with pulsed two-dimensional transducer arrays, IEEE Trans. Ultrason. Ferroelectrics Frequency Control 38 (1991) 320–333.
[7] P.N.T. Wells, The present status of ultrasonic imaging in medicine, Ultrasonics 31 (1993) 345–351.
[8] A.E. Weyman, Principles and Practice of Echocardiography, Lea and Febiger, Philadelphia, 1994.
[9] M.T. Buchanan, K. Hynynen, Design and experimental evaluation of an intracavity ultrasound phased array system for hyperthermia, IEEE Trans. Biomed. Eng. 41 (1994) 1178–1187.
[10] H. Wang, E.S. Ebbini, M. O'Donnell, C.A. Cain, Phase aberration correction and motion compensation for ultrasonic hyperthermia phased arrays: experimental results, IEEE Trans. Ultrason. Ferroelectrics Frequency Control 41 (1994) 34–43.
[11] Y.J. Yoon, P.J. Benkeser, Ultrasonic phased arrays with variable geometric focusing for hyperthermia applications, IEEE Trans. Ultrason. Ferroelectrics Frequency Control 39 (1992) 273–278.
[12] J.-L. Thomas, M.A. Fink, Ultrasonic beam focusing through tissue inhomogeneities with a time reversal mirror: application to transskull therapy, IEEE Trans. Ultrason. Ferroelectrics Frequency Control 43 (1996) 1122–1129.
[13] W. Gerbhardt, Improvement of ultrasonic testing by phased arrays, Nucl. Eng. Design 76 (1983) 275–283.
[14] M. Gottlieb, C.L.M. Ireland, J.M. Ley, Electro-Optic and Acousto-Optic Scanning and Deflection, Marcel Dekker Inc, New York, 1983, 101, 150–156.
[15] R. Huang, L.W. Schmerr, A. Sedov, Modeling the radiation of ultrasonic phased-array transducers with Gaussian beams, IEEE Trans. Ultrason. Ferroelectr. Freq. Control 55 (2008) 2692–2702.
[16] D.J. Vezzetti, Propagation of bounded ultrasonic beams in anisotropic media, J. Acoust. Soc. Am. 78 (1985) 1103–1108.
[17] L.W. Schmerr, Fundamentals of Ultrasonic Nondestructive Evaluation, Plenum Press, New York, 1998, p. 543.
[18] X. Zhao, T. Gang, Nonparaxial multi-Gaussian beam models and measurement models for phased array transducers, Ultrasonics 49 (2009) 126–130.
[19] T. Wang, C. Zhang, A. Aleksov, I. Salama, A. Kar, Effect of large deflection angle on the laser intensity profile produced by acousto-optic deflector scanners in high precision manufacturing, J. Laser Appl. 28 (2016), 12012–1:8.

[20] T. Wang, C. Zhang, A. Aleksov, I. Salama, A. Kar, Dynamic two-dimensional refractive index modulation for high performance acousto-optic deflector, Opt. Express 23 (2015) 33667–33680.
[21] Kazuyuki Nakahata, Naoyuki Kono, in: Santos (Ed.), 3-D Modelings of an Ultrasonic Phased Array Transducer and Its Radiation Properties in Solid, Ultrasonic Waves, InTech, 2012, pp. 60–80, ISBN: 978-953-51-0201-4. Available from: <http://www.intechopen.com/books/ultrasonic-waves/3-d-modelings-of-an-ultrasonic-phased-array-transducer-and-its-radiation-properties-in-solid>.
[22] M.G. Silk, Ultrasonic Transducers for Nondestructive Testing, Adam Hilger Ltd, Bristol, 1984, pp. 76–84, 90–93.
[23] L.N.G. Filon, Proc. Roy. Soc. Edinburgh 49 (1928) 38–47.
[24] A.K. Rigler, Note on the fast Fourier transform, J. Optical Soc. Am. 58 (1968) 274–275.
[25] M. Abramowitz, I.A. Stegun, Handbook of Mathematical Functions: With Formulas, Graphs, and Mathematical Tables, Dover Publications Inc, 1964, pp. 231–233.
[26] N. Uchida, Y. Ohmachi, Elastic and photoelastic properties of TeO_2 single crystal, J. Appl. Phys. 40 (1969) 4692–4695.
[27] J.W. Goodman, Introduction to Fourier optics, Roberts and Company Publishers (2005) 84–88.